A Simple Route to the Synthesis of Core/Shell Nanoparticles of Chalcogenides

M. Azad Malik,[†] Paul O'Brien,*[,†] and Neerish Revaprasadu[‡]

The Manchester Materials Science Centre and the Department of Chemistry, Manchester University, Oxford Road, Manchester M13 9PL, United Kingdom, and Department of Chemistry, University of Zululand, Private Bag X1001, Kwadlangezwa, 3886 South Africa

Received June 25, 2001. Revised Manuscript Received December 4, 2001

In this work, we report the synthesis of CdSe/CdS, CdSe/ZnS, and CdSe/ZnSe core/shell and CdSe/CdS alloy nanoparticles using bis(hexyl(methyl)dithio-/-diselenocarbamato)-cadmium(II)/zinc(II) compounds as single-source precursors. We compare the optical properties of the core/shell nanoparticles in relation to those of the parent organically capped binary nanoparticles. We also compare the properties of CdSe alloys to those of the CdSe particles and core/shell structures. The absorption spectra of CdSe/CdS, CdSe/ZnS, and CdSe/ZnSe show red shifts of 0.020, 0.038, and 0.046 eV, respectively, with respect to the parent CdSe nanoparticles. Photoluminescence spectra ($\lambda_{exc} = 400$ nm) CdSe/CdS (622 nm), CdSe/ZnS (620 nm), and CdSe/ZnSe (617 nm) show emissions close to the absorption band edge. The emission maximum of the core/shell materials shows red shifts in relation to the emission maximum of CdSe consistent with the red shifts in the absorption spectra. The intensity of the emission maximum is considerably increased in the core/shell structure as compared to the parent materials. The X-ray diffraction pattern of the CdSe−CdS composite are broad and poorly defined. The HRTEM micrographs of the core/shell nanoparticles show well-defined, spherical particles with larger diameters than the particles of the parent material.

Introduction

The high surface-to-volume ratio of nanocrystalline semiconductors means that their surfaces play an important role in their electronic and optical properties. It is for this reason that surface modification of these particles has been the subject of extensive investigation. Passivation has been achieved by the capping of the nanocrystallites with organic and inorganic materials. In colloidal CdS, surface defects have been passivated by $Cd(OH)_2$, with a dramatic increase in fluorescence reported in the surface-modified sample.[1] Organic ligands such as thiopyridines[2] and thiolates[3] have also been reported to minimize surface defects and increase luminescence efficiencies.

The growth of a shell of a second material on a core of another material to form a heterostructure has been a successful route in the surface modification of nanostructured particles. In the colloidal synthesis of these structures the core acts as a seed for the heterogeneous nucleation of the shell. Core/shell systems reported include Si/SiO_2,[4] $CdS/Cd(OH)_2$,[1] CdSe/ZnS,[5,6] ZnS/CdS,[7] CdS/HgS,[8] HgS/CdS,[9] CdS/PbS,[10] CdSe/ZnSe,[11,12] and CdSe/CdS,[13−15] with accounts of improved luminescence quantum yields, decreased fluorescence lifetimes, and benefits related to the tailoring of relative band gap positions between the two materials. Recently, Mulvaney et.al.[16] reported the encapsulation of metal clusters and semiconductor by silica shells. The silica shell allows for stabilization against photochemical degradation and high fluorescence quantum yields.

In this work, we report the synthesis of CdSe/CdS,[17] CdSe/ZnS and CdSe/ZnSe core/shell nanoparticles using bis(hexyl(methyl)dithio-/diselenocarbamato)cadmium-(II)/zinc(II) compounds as single-source precursors. In addition, we report the synthesis of CdSe−CdS composites.

* Corresponding author: Professor Paul O'Brien, Department of Chemistry, Manchester University, Oxford Rd, Manchester M13 9PL, U.K.

[†] Manchester University.

[‡] University of Zululand.

(1) Spanhel, L.; Haase, M.; Weller, H.; Henglein, A. *J. Am. Chem. Soc.* **1987**, *109*, 5649.

(2) Katari, J. E.; Colvin, V. L.; Alivisatos, A. P. *J. Phys. Chem.* **1994**, *98*, 4109.

(3) Noglik, H.; Pietro, W. J. *Chem. Mater.* **1994**, *6*, 1593.

(4) Wilson, W. L.; Szajowsk, P. F.; Brus, L. E. *Science* **1993**, *262*, 1242.

(5) Kortan, A. R.; Hull, R.; Opila, R. L.; Bawendi, M. G.; Steigerwald, M. L.; Carrol, P. J.; Brus, L. E. *J. Am. Chem. Soc.* **1990**, *112*, 1327.

(6) Hines, M. A.; Guyot-Sionnest, P. *J. Phys. Chem.* **1996**, *100*, 468.

(7) Weller, H.; Koch, U.; Gutierrez, M.; Henglein, A. *Ber. Bunsen-Ges. Phys. Chem.* **1987**, *91*, 88.

(8) Hasselbarth, A.; Eychmuller, A.; Eichburger, R.; Giesi, M.; Mews, A.; Weller, H. *J. Phys. Chem.* **1993**, *97*, 5333.

(9) Hasselbarth, A.; Eychmuller, A.; Weller, H. *J. Lumin.* **1992**, *53*, 112.

(10) Zhou, H. S.; Honma, I.; Sasahara, H.; Komiyama, H.; Kraus, J. W. *Chem. Mater.* **1994**, *6*, 1534.

(11) Kortan, A. R.; Hull, R.; Opila, R. L.; Bawendi, M. G.; Steigerwald, M. L.; Carrol, P. J.; Brus, L. E. *J. Am. Chem. Soc.* **1990**, *112*, 1327.

(12) Danek, M.; Jensen, K. F.; Murray, C. B.; Bawendi, M. G. *Chem. Mater.* **1996**, *8*, 173.

(13) Peng, X.; Schlamp, M. C.; Kadavanich, A. V.; Alivisatos, A. P. *J. Am. Chem. Soc.* **1997**, *119*, 7019.

(14) Tian, Y.; Newton, T.; Kotov, N. A.; Guldi, D. M.; Fendler, J. H. *J. Phys. Chem.* **1996**, *100*, 8927.

(15) Banin, U.; Bruchez, M.; Alivisatos, A. P.; Ha, T.; Weiss, S.; Chemla, D. S.*J. Chem. Phys.* **1999**, *110*, 1195.

(16) Mulvaney, P.; Liz-Marzan, L. M.; Giersig, M.; Ung, T. *J. Mater. Chem.* **2000**, *10*, 1259.

(17) Revaprasadu, N.; Malik, M. A.; O'Brien, P.; Wakefield, G. *J. Chem. Soc., Chem. Commun.* **1999**, 1573.

10.1021/cm011154w CCC: $22.00
Published on Web 04/05/2002

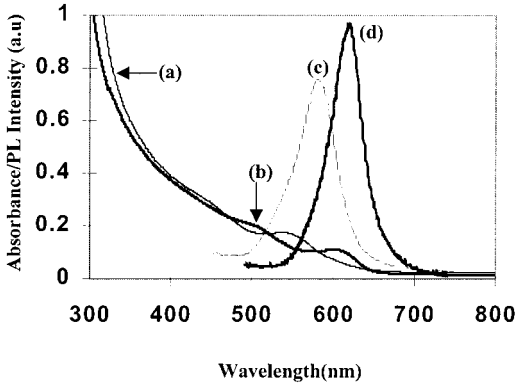

Figure 1. Absorption spectra of (a) CdSe and (b) CdSe/CdS core/shell nanoparticles and photoluminescence spectra (λ_{exc} = 400 nm) of (c) CdSe and (d) CdSe/CdS nanoparticles.

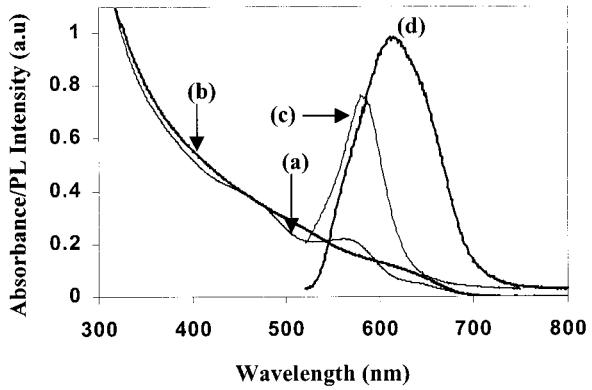

Figure 2. Absorption spectra of (a) CdeSe and (b) CdSe/ZnS core/shell nanoparticles and photoluminescence spectra (λ_{exc} = 400 nm) of (c) CdSe and (d) CdSe/ZnS core/shell nanoparticles.

Experimental Section

Chemicals. Cadmium acetate, *N*-methylhexylamine, selenium, zinc acetate, zinc hydroxide, tri-*n*-octylphosphine (TOP), and tri-*n*-octylphosphine (TOPO) were purchased from Aldrich Chemical Company Ltd. Carbon disulfide, 1,4-dioxane, methanol, and toluene were obtained from BDH. The solvents used for air-sensitive chemistry were distilled, deoxygenated under a nitrogen flow and stored over molecular sieves (type 4 Å, BDH) before use. TOPO was purified by vacuum distillation at ca. 250 °C (0.1 Torr). The purity of TOPO was checked by ^{1}H NMR spectroscopy and melting point measurement (54 °C).

UV/Vis and IR Spectroscopy. A Philips PU 8710 spectrophotometer was used to carry out optical measurements, with samples placed in silica cuvettes (1-cm path length). The optical measurements were carried out using toluene as the reference.

The "optical band gaps" (E_g's) of the nanodispersed materials were determined by fitting the absorption edge data to a direct transition process. E_g was obtained by extrapolation following a linear regression on the absorption band edge data (R^2 for the fit not less than 0.98). Infrared spectra were carried out using a Matteson Polaris FT-IR spectrometer with the samples as Nujol mulls.

Photoluminescence Spectroscopy. A Spex FluoroMax instrument with a xenon lamp (150 W) and a 152 P photomultiplier tube as the detector was used to measure the photoluminescence of the particles. Good spectra were obtained with the slits set at 2 nm and an integration time of 1 s. The samples were placed in quartz cuvettes (1-cm path length). The wavelength of excitation is indicated in the text and was shorter than the onset of absorption of the particular sample being studied.

X-ray Diffraction (XRD). X-ray diffraction patterns were measured on a Philips PW 1700 series automated powder diffractometer using Cu K_α radiation at 40 kV and 40 mA with a secondary graphite crystal monochromator. Samples were supported on glass slides (5 cm). A concentrated suspension of the particles was slowly evaporated at room temperature onto a glass slide to obtain a sample for analysis. X-ray diffraction patterns on samples were performed using secondary graphite-monochromated Cu K_α radiation (40 kV) on a Philips X'Pert Materials Research Diffractometer. Measurements were taken using a glancing-angle incidence detector at an angle of 3° for 2θ values in the range 20−60° in steps of 0.04° with a count time of 1 s.

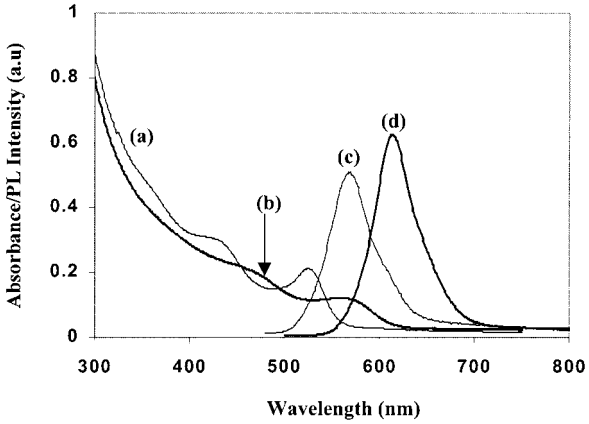

Figure 3. Absorption spectra of (a) CdSe and (b) CdSe/ZnSe core/shell nanoparticles and photoluminescence spectra (λ_{exc} = 400 nm) of (c) CdSe and (d) CdSe/ZnSe core/shell nanoparticles.

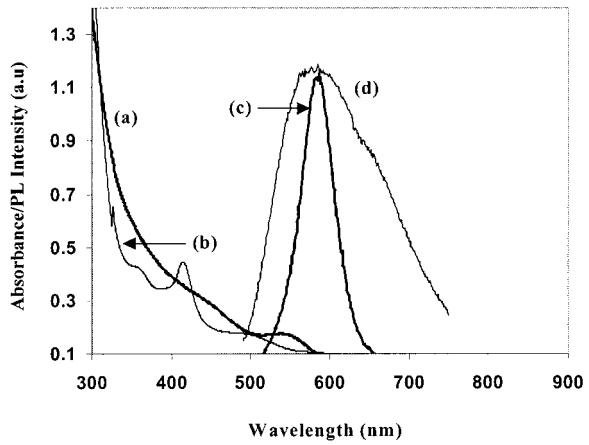

Figure 4. Optical spectra of the CdSe−CdS composites and CdSe including absorption spectra of (a) CdSe and (b) CdSe−CdS and PL spectra of (c) CdSe and (d) CdSe−CdS.

Electron Microscopy. A Joel 2000 FX MK 1 electron microscope operated at 200 kV with an Oxford Instruments AN 10000 EDS analyzer was used for the conventional TEM (transmission electron microscopy) images. Selected area electron diffraction (SAED) patterns were obtained using a JEOL 2000 FX MK2 electron microscope operated at 200 kV. The samples for TEM and SAED were prepared by placing a drop of a dilute solution of sample in toluene on a copper grid (400 mesh, agar). The excess solvent was wicked away with a paper tip, and the sample was allowed to dry completely at room temperature.

EDAX (energy dispersion analytical X-ray) was performed on samples deposited by evaporation onto glass substrates using a JEOL JSM35CF scanning electron microscope. For the HRTEM images, a drop of a dilute solution of sample was placed on a holey carbon film, left to evaporate, and then examined in a JEOL 4000EX TEM at 400 kV.

Synthesis of Bis(hexyl(methyl)dithio-/diselenocarbamato)cadmium(II)/zinc(II). Bis(hexyl(methyl)dithio-/dis-

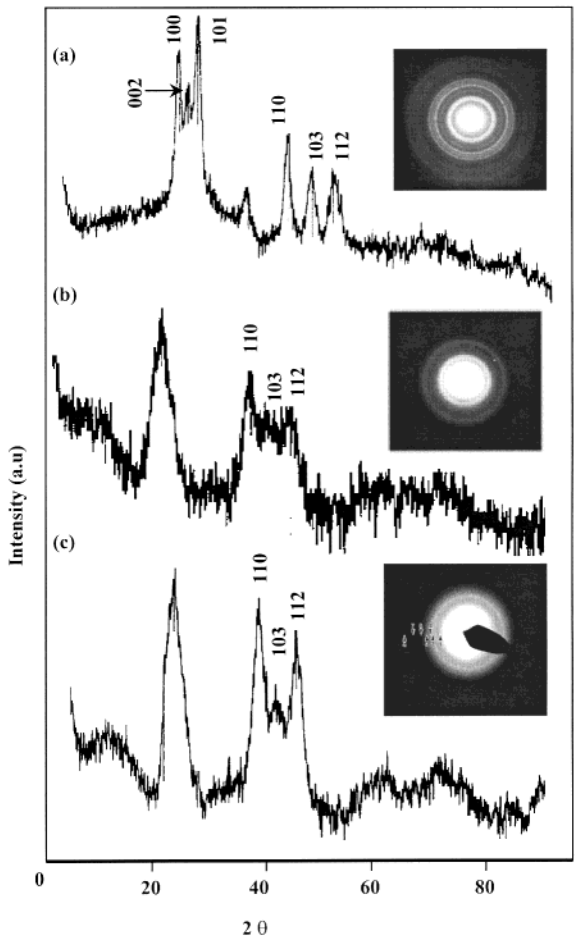

Figure 5. XRD and SAED patterns of (a) CdS, (b) CdSe, and (c) CdSe/CdS core/shell nanoparticles.

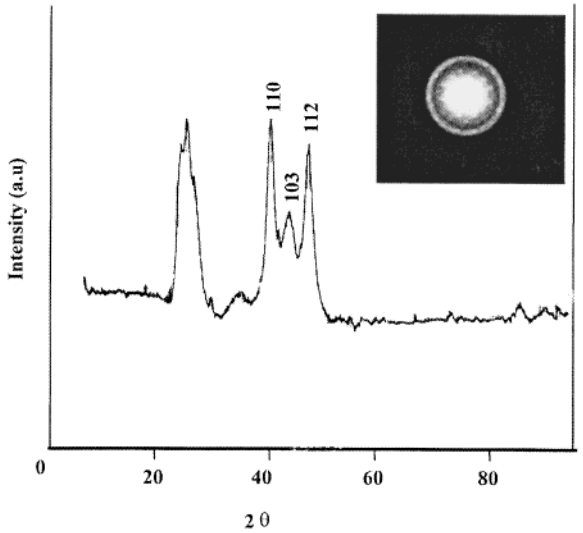

Figure 6. XRD and SAED patterns of CdSe/ZnS core/shell nanoparticles.

elenocarbamato)cadmium(II)/zinc(II) were prepared by the methods described in a previous paper.[18]

Synthesis of CdSe and CdS Nanoparticles. CdS and CdSe nanocrystals were synthesized as described previously.[17,19,20]

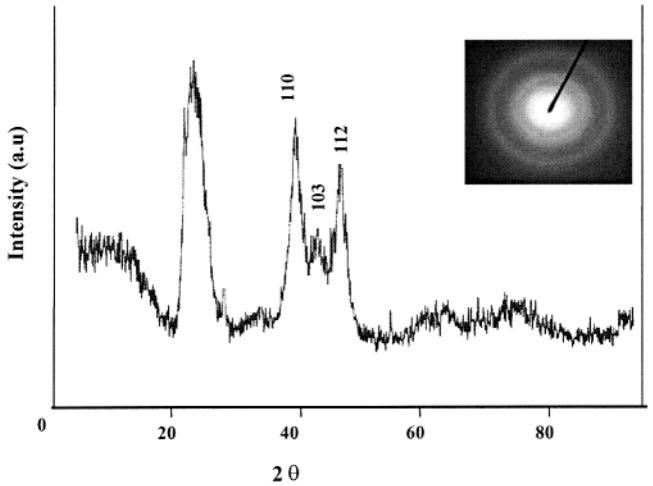

Figure 7. XRD and SAED patterns of CdSe/ZnSe core/shell nanoparticles.

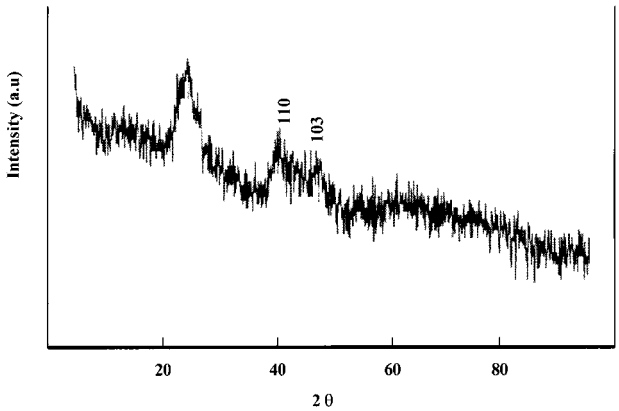

Figure 8. XRD pattern of CdSe−CdS composites.

Synthesis of Core/Shell Nanoparticles. *CdSe/CdS.* In a typical synthesis, $Cd[Se_2CNMe(Hex)]_2$ (0.8 g) was dissolved in trioctylphosphine (TOP) (15 mL). This solution was then injected into hot (250 °C) tri-*n*-octylphosphine oxide (TOPO) (20 g) and kept at this temperature for 30 min to give CdSe. To prepare the core/shell structure, a solution of $Cd[S_2CNMe(Hex)]_2$ (0.5 g) in TOP (10 mL) was injected into the deep red reaction mixture. The reaction was allowed to proceed for an additional 30 min, and the resulting solution was cooled to ca. 70 °C. Methanol was then added, and a flocculant precipitate formed that was separated by centrifugation.

CdSe/ZnS and CdSe/ZnSe. The above procedure was repeated to prepare the CdSe/ZnS and CdSe/ZnSe core/shell nanoparticles, using $Zn(S_2CNMeHex)_2$ and $Zn(Se_2CNMeHex)_2$ as the precursors for the shells.

Synthesis of CdSe−CdS Composites. The CdSe−CdS composites were prepared by dissolving $Cd(Se_2CNMeHex)_2$ and $Cd(S_2CNMeHex)_2$ (0.5 g) in TOP. This solution was injected into hot (250 °C) TOPO and kept at this temperature for 45 min. The posttreatment carried out was similar to that of the core/shell nanoparticles, with the resultant isolated particles being dissolved in toluene.

Results and Discussion

Optical Properties. The growth of a shell around a core nanoparticle modifies the optical properties of the nanoparticle. The difference in the optical properties of the core/shell particles in comparison with those of the

(18) Motevalli, M.; O'Brien, P.; Walsh, J. R.; Watson, I. M. *Polyhedron* **1996**, *15*, 2801.

(19) Ludolph, B.; Malik, M. A.; Revaprasadu, N.; O'Brien. P. *J. Chem. Soc., Chem. Commun.* **1998**, 1849.

(20) Malik, M. A.; Revaprasadu, N.; O'Brien, P. *J. Mater. Chem.* **2001**, *13*, 913.

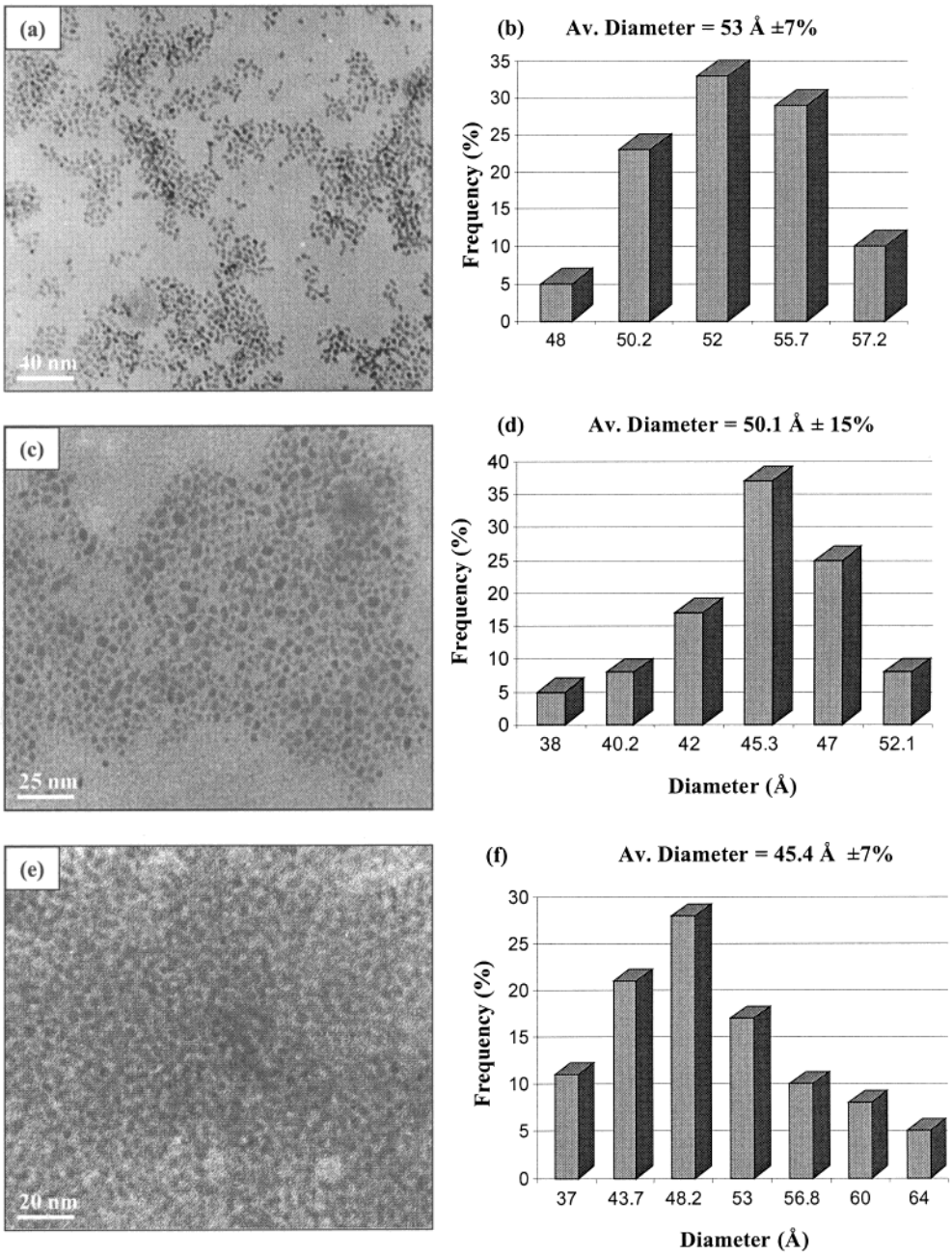

Figure 9. TEM micrographs of (a) CdSe/CdS, (c) CdSe/ZnSe, and (e) CdSe/ZnSe and their corresponding (b, d, f) average particle size distributions.

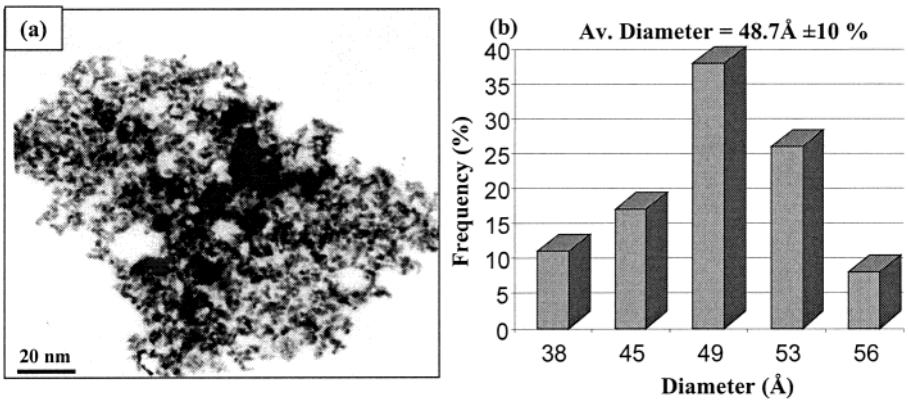

Figure 10. CdSe/CdS composite nanoparticles (a) TEM image and (b) particle size distribution.

bare nanoparticles is evidence of shell growth. In this work, we compare the optical properties of the core/shell nanoparticles in relation to those of organically capped CdSe nanoparticles. We also compare the properties of

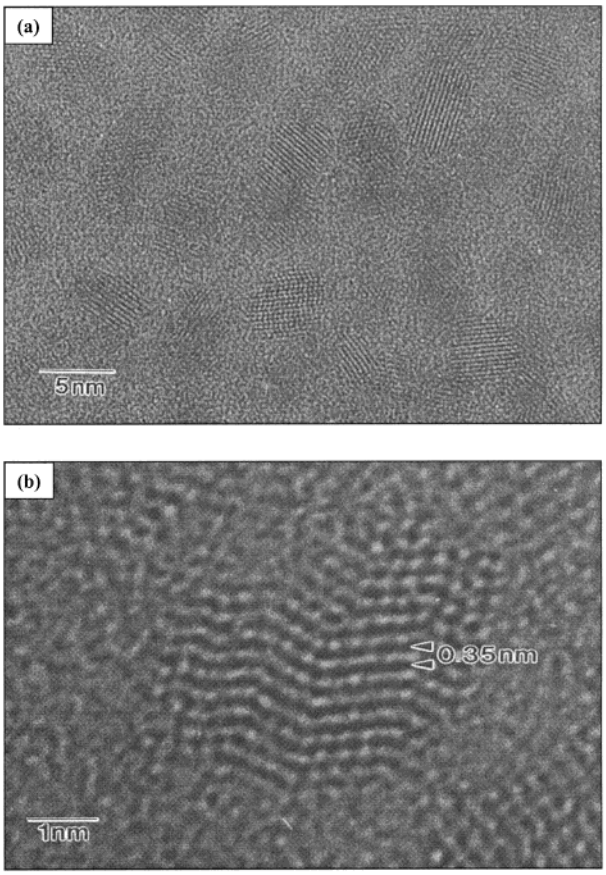

Figure 11. HRTEM images of CdSe/CdS core/shell nanoparticles showing (a) an array of nanoparticles and (b) a single quantum dot (diameter = ca. 4 nm).

simple composites of CdSe−CdS with those of CdSe particles.

The absorption spectra for CdSe and CdSe/CdS nanoparticles are shown in Figure 1. The band edge of CdSe/CdS is at 652 nm (1.90 eV), a red shift of 22 nm (0.02 eV) compared to that of CdSe (630 nm, 1.92 eV). This red shift is indicative of the formation of the core/shell structure. The overall shape of the spectrum is similar to that of CdSe; however, a slight sharpening of the features at 535 and 613 nm is observed, which might suggest a narrower size distribution.

A red shift is also observed in the absorption spectra of CdSe/ZnS and CdSe/ZnSe nanoparticles. The absorption spectrum of the CdSe/ZnS nanoparticles shows less-defined features as compared to that of CdSe (Figure 2). The excitonic features at 450 and 550 nm in the CdSe absorption spectra are smoothed out in the CdSe/ZnS spectrum. Peng et al.[13] reported similar observations in the absorption spectra of CdSe/CdS nanoparticles whereby the overall shape of the spectrum was maintained, with a broadening of the excitonic features as the band edge shifted to lower energy. This broadening effect was also observed in the absorption spectra of CdSe/CdS and CdSe/ZnSe nanoparticles (Figure 3). However, the enhanced effect in the CdSe/ZnS absorption spectrum could be due to a broad size distribution. The band edge (670 nm, 1.85 eV) of CdSe/ZnS is red-shifted by 47 nm (0.038 eV) in relation to that of CdSe (623 nm, 1.99 eV). A red shift of 57 nm (0.046 eV) is observed for CdSe/ZnSe (630 nm, 1.97 eV) as compared to CdSe (563 nm, 2.20 eV). The red shifts in the absorption spectra of the core/shell nanoparticles in relation to the parent material are attributed to relaxation of quantum confinement resulting from the growth of the shell.[12] XRD and TEM confirm this increase in particle size. The broadening of the second absorption band in CdSe/ZnS (570 nm) and CdSe/ZnSe (520 nm) is also due to surface passivation by the inorganic shell, as the second excited state has more electron density close to the particle surface so that its energy should be more sensitive to surface derivatization.[12]

The photoluminescence spectra (λ_{exc} = 400 nm) of CdSe/CdS, CdSe/ZnS, and CdSe/ZnSe show emissions close to the absorption band edge. The emission maximum of CdSe/CdS is at 622 nm, with that of CdSe/ZnS at 620 nm and that of CdSe/ZnSe at 617 nm. The emission maxima of the core/shell materials show red shifts in relation to the emission maximum of CdSe, consistent with the red shifts visible in the absorption spectra. More importantly, the intensity of the emission maximum, which is normalized to the absorption spectrum, is considerably increased in the core/shell structure as compared to the parent materials (CdSe). This enhanced emission has been reported previously for various core/shell structures.[1−15]

The emission spectrum of CdSe/ZnS is broad, indicating a wide size distribution, as confirmed by the shape of the absorption spectrum. This observation is probably due to Ostwald ripening; however, it is very difficult to explain because the reaction conditions did not vary from those used for CdSe/CdS and CdSe/ZnSe. There is no evidence of deep-trap emission in any of the PL spectra.

The absorption spectrum of the CdSe−CdS composites shows a sharp excitonic feature at 417 nm with the absorption band edge at 584 nm (2.12 eV) (Figure 4). The blue shift of 46 nm (0.037 eV) in relation to CdSe is indicative of alloying.[12,13] The PL spectrum (λ_{exc} = 400 nm) of the composite shows an emission maximum (588 nm), a value close to band edge emission. The emission spectrum is broader than that of CdSe; however, the sharp band edge and the observed size distribution from the TEM micrographs suggest a narrow size distribution.

Structural Characteristics. The XRD patterns of CdSe/CdS (Figure 5), CdSe/ZnS (Figure 6), and CdSe/ZnSe (Figure 7) show broad peaks along the (110), (103), and (112) planes that are assigned to the hexagonal phase of CdSe, suggesting that the diffraction is predominantly due to CdSe core. The X-ray data could be consistent with a core/shell structure or with the formation of a composite, but the composite would give a blue shift in the emission and absorption edge. The red shift in the absorption spectra shows that the core/shell structure is formed. CdSe and ZnS do not alloy well because of their large lattice mismatch, whereby the Cd−Se (6.05 Å) lattice is about 12% larger than the Zn−S (5.41 Å) lattice.[6]

The X-ray diffraction patterns of the core/shell structures show the lattice parameters between the CdSe core and the CdS/ZnS/ZnSe shell, which correspond to the observation by Peng et al.[21] that, as the thickness

(21) Peng, X.; Schlamp, M. C.; Kadavanich, A. V.; Alivisatos, A. P. *J. Am. Chem. Soc.* **1997**, *119*, 7019.

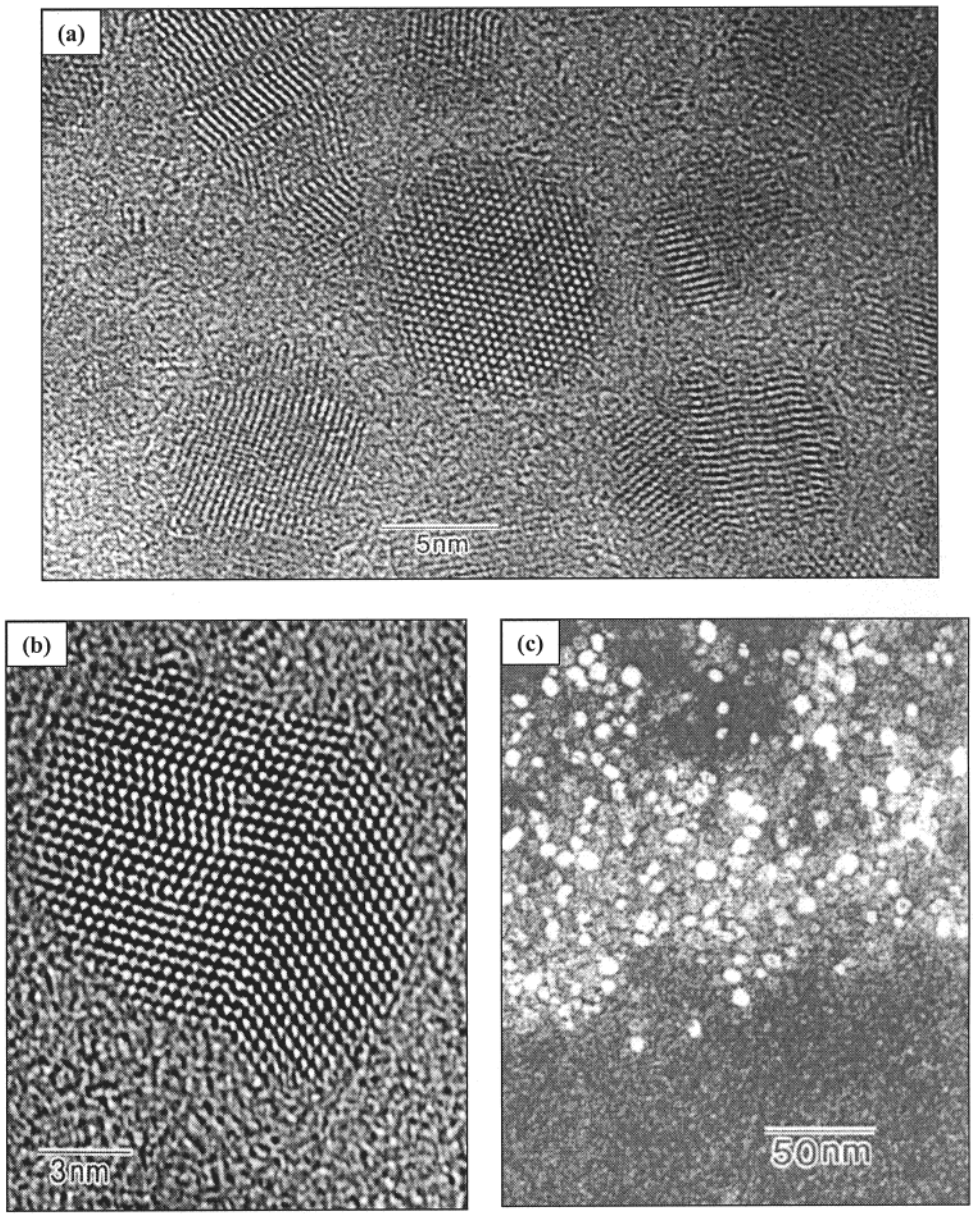

Figure 12. CdSe/ZnS core/shell nanoparticles: (a) HRTEM image showing an array of particles, (b) HRTEM image of single quantum dot showing grain boundaries, and (c) bright-field TEM image.

of the shell increases in CdSe/CdS core/shell materials, the peak shift increases toward higher angle, i.e., from the CdSe pattern toward the CdS pattern. Similarly, in the comparison of the SAED patterns, the CdSe/CdS pattern is intermediate between that for CdS and that for CdSe as expected (Figure 5). The peaks along the (002), (100), and (101) planes shown in the hexagonal CdS diffraction pattern are not visible in the CdSe, CdSe/CdS, CdSe/ZnS, and CdSe/ZnSe patterns because of the broadening of the peak in the region $d\theta \approx 20-25°$. The X-ray diffraction of the CdSe−CdS composite shows broad, poorly defined peaks along the (110) and (103) planes (Figure 8). The peak broadening could be due to the presence of defects in the crystal lattice. The shift in the peaks to lower 2θ values and the blue shift in the absorption spectrum are evidence for composite formation.

TEM images and particle size distribution histograms for CdSe/CdS, CdSe/ZnS, and CdSe/ZnSe core/shell nanoparticles are shown in Figure 9. The TEM micrographs of the core/shell nanoparticles show well-defined, spherical particles with an increase in diameter as compared to the parent material. The CdSe/CdS nanoparticles have an average particle size diameter of 53 Å ± 7%, an increase of 8 Å in relation to CdSe (45 Å ± 5%). CdSe/ZnS (50.1 Å ± 15%) shows an increase of 9.1 Å and CdSe/ZnSe (45.4 Å ± 7%) an increase of 6.9 Å in relation to the parent material. This increase in particle size diameter is due to the growth of the shell. This is consistent with the observed broadening of the absorption band edge in the core/shell nanoparticles. In CdSe/ZnS, the particle size distribution increases dramatically from 5% in CdSe to 15% upon shell growth. This broad size distribution is clearly confirmed by the broadened absorption band edge and broad photoluminescence spectrum of CdSe/ZnS.

The TEM image of the CdSe−CdS composites shows particles with an average size of 48.7 Å (±10%) (Figure 10a). The "darker" particles appearing in the micrograph are indicative of a dense agglomeration of par-

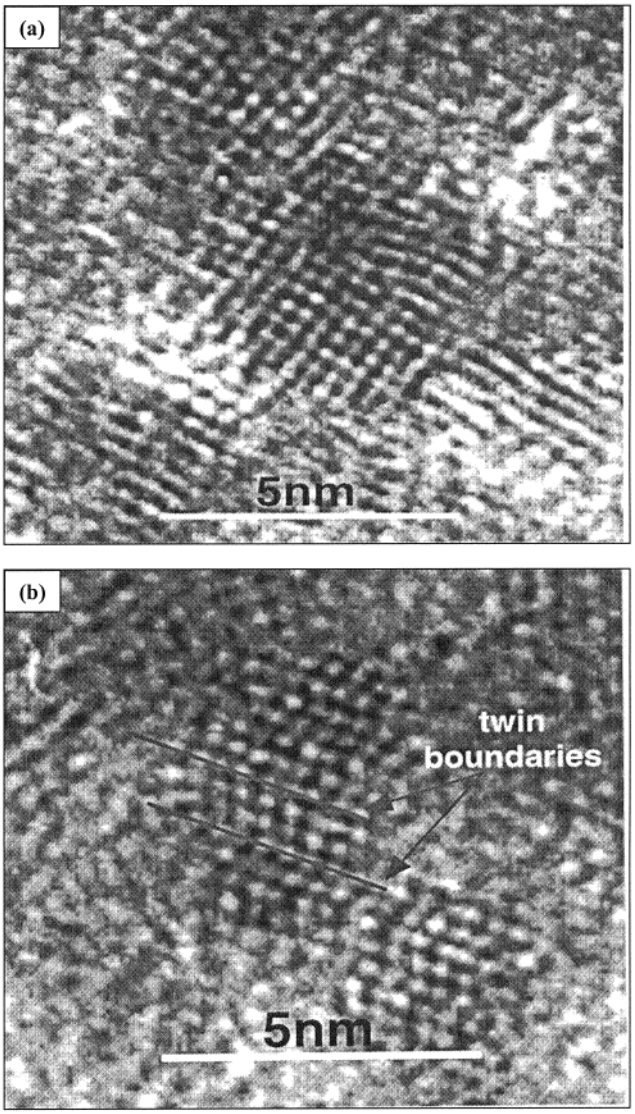

Figure 13. HRTEM images of CdSe/ZnSe core/shell showing (a) stacking faults and (b) twin boundaries.

ticles. The standard deviation (±10%) is higher than that of the core/shell samples (±7%); however, this factor alone cannot account for the broad emission spectrum. The EDAX pattern confirmed the presence of Cd, Zn, Se, and S in the core/shell and composite nanoparticles. The peak for phosphorus in the EDAX spectrum in each case was due to the capping of the particles by TOPO. The ICP-AES analysis of cadmium shows an increase in cadmium from CdSe (35.6%) to CdSe/CdS core/shell (composite) [46.3% (38.9%)] and then a decrease for CdSe/ZnS core/shell (composite) [29.6% (24.4%)] and CdSe/ZnSe core/shell (composite) [24.6% (20.9%)], as expected.

The crystallinity of the core/shell nanoparticles was confirmed by the clear lattice fringes for the CdSe core as observed by HRTEM (Figures 11−13) In CdSe/CdS (Figure 11), the lattice spacing is intermediate between those of CdSe and CdS, as indicated by SAED and X-ray diffraction patterns. The lattice fringes persist throughout the entire nanocrystal, an indication of epitaxial growth.

As expected, HRTEM revealed no clear interface between the core and shell. The nanoparticles were faceted consistent with previous observations on CdSe nanoparticles.[13] HRTEM images of single particles show that defects are present. In CdSe/CdS (Figure 11b) and CdSe/ZnSe (Figure 13a), stacking faults are clearly evident with dislocations also visible in CdSe/ZnS (Figure 13b). These stacking faults are the predominant forms of disorder in bulk II/VI materials.[22] CdSe and CdSe/CdS core/shell nanoparticles were also reported to display stacking faults.[13] Twin rotational faults also appear in CdSe/ZnSe, with the twin boundaries visible in Figure 13b. The stacking faults extend across the entire nanoparticle, suggesting that any stacking faults present initially in the core are passed on to the shell during shell growth. Although the hexagonal phase of the crystalline core is dominant, there is also evidence from the HRTEM images that there is a degree of phase change to the cubic phase. This change in phase could be responsible for the stacking faults.

Conclusion

CdSe/CdS, CdSe/ZnS, CdSe/ZnSe core/shell structures and CdSe−CdS composites have been synthesized from bis(hexyl(methyl)dithio-/-diselenocarbamato)cadmium-(II)/zinc(II) precursors and their optical and structural properties discussed.

The absorption and emission spectra of core/shell structures show red shifts as compared to the parent materials which indicates the formation of core/shell structures. In contrast, CdSe−CdS composite gives blue shifts in its absorption and emission spectra as expected. More importantly, the intensity of the emission maximum, which is normalized to the absorption spectrum, is considerably increased in the core/shell structure as compared to the parent materials. The XRD patterns of all core/shell structures give broad peaks along the (110), (103), and (112) planes that are assigned to the hexagonal phase of CdSe, suggesting that the diffraction is predominantly due to the CdSe core. X-ray diffraction of the CdSe−CdS composite shows broad, poorly defined peaks along the (110) and (103) planes. The shift in the peaks to lower 2θ values and the blue shift in the optical spectra are evidence for composite formation. The TEM micrographs of the core/shell nanoparticles show well-defined, spherical particles with an increase in diameter compared to the parent material.

Acknowledgment. We thank the Royal Society and the National Research Foundation (NRF) for support to N.R. and a program of collaboration between UZULU and ICSTM. P.O.B. thanks the EPSRC for a grant. P.O.B. is the Sumitomo/STS Visiting Professor of Materials Chemistry at IC. We thank G. Wakefield, Department of Engineering Science, University of Oxford, for HRTEM assistance.

CM011154W

(22) Murray, C. B.; Norris, D. J.; Bawendi, M. G. *J. Am. Chem. Soc.* **1993**, *115*, 8706.